M2 de Biophysique Moléculaire et Cellulaire
Cours N°3: Analyse Bidimensionnelle d'Images de Particules Isolées

Nicolas BOISSET et Slavica JONIC

Département de Biologie Structurale de l'IMPMC

Institut de minéralogie et de physique des milieux condensés

CNRS UMR 7590, Universités Paris 6, Paris 7, IPGP

140 Rue de Lourmel, 75015 Paris

Tel. (S. JONIC): 01 44 27 72 05

URL: http://www.impmc.jussieu.fr

- Numérisation de l'image, cameras CCD
- Sélection des particules et normalisation du contraste
- Alignement
- Classification des images

Numérisation de l' image

Les détecteurs CCD ont révolutionné la cristallographie X, et commencent a pouvoir remplacer les films photographiques pour certaines applications de la cryoMET.

Numérisation de l'image : Une partie d'un cours donné par Helen Saibil et Elena Orlova au cours EMBO 2003.

Lecture 4

H. Saibil
Sept 2003

EMBO Practical Course on
Image processing for cryo EM

Lecture 4

Optical density

Optical density (OD) is the logarithm of the transmittance (transparency) of the film

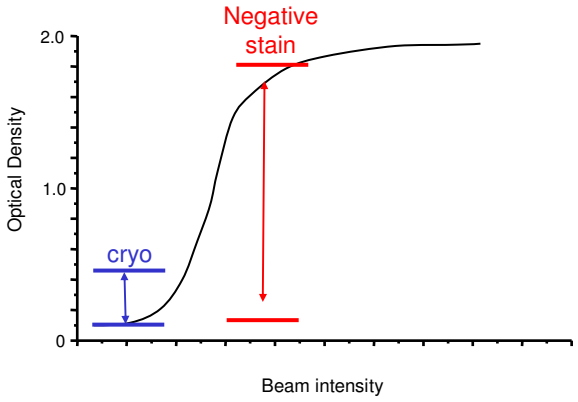

The range of optical densities in cryo EM images is very limited

Lecture 4

Film scanners

Spot scanning (Joyce-Loebl/Perkin Elmer) - incredibly slow and accurate. Can do 5 μm, spot formed by microscope objective lens, transmittance measured relative to a reference beam. 8h to scan a negative at high resolution. Isotropic in xy resolution - lens moved by accurate stepper motors. Huge.

Drum – (Optronics, Heidelberg Tango) Optics good, mechanics not as good, relatively quick, no reference beam

CCD – (Zeiss SCAI, Nikon Coolscan) Very quick and less accurate. Patch or strip of CCD elements moves relative to film, resolution different in x and y; some geometrical distortion; more noisy measurement; amplitude loss at high resolution

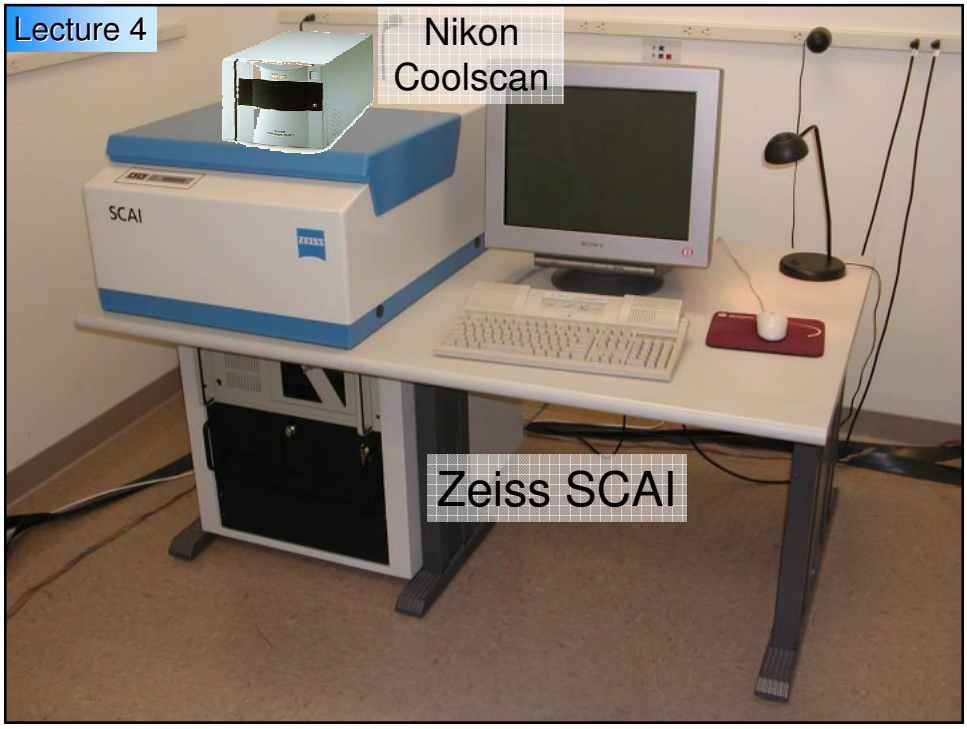

Lecture 4

Criteria for evaluating film scanners

Geometric accuracy: Scan of regular grid at 0 and 90° orientations

DQE: digital quantum efficiency - $(SNR)^2$ (signal to noise ratio) of scan divided by $(SNR)^2$ of image.

MTF: modulation transfer function - like the CTF, amplitude of signal transmitted by scanner as a function of resolution, but no phase changes

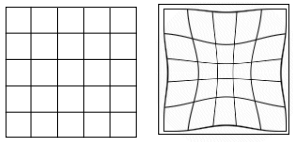

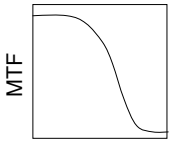

Lecture 4

Digital images

Image Digitization

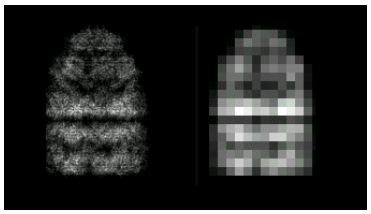

Original image

Image sampled at low resolution

Each picture element stored in the computer, with its own grey level, is called a **pixel**.

Pixel grey levels: black to white is 0-255 for an 8-bit image.

Pixel size

The image must be divided up into pixels (sampled) at a spacing at least twice as fine as the finest detail (highest frequency) to be analysed.
(in practice, 3-4x as fine).

Computer storage

Fineness of grid ($512^2 = 262144$)
No. of different gray levels:
e.g. 0-7, 0-63, 0-255
$2^8 = 256$, 8 bits or 1 byte

Lecture 4

Sampling

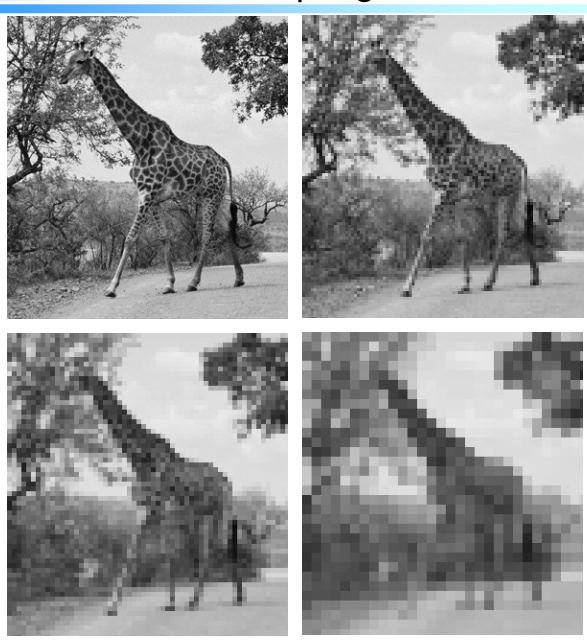

Lecture 4

Sampling - spatial resolution

Remember that the image can be represented as the sum of a series of sinusoidal waves. The highest frequency wave term present defines the resolution limit. When an image is digitised, the wave components are sampled at an interval defined by the scanner step size.

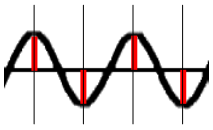

Nyquist frequency: the sampling frequency is twice the highest frequency term being represented.

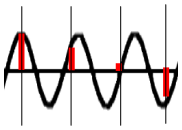

If the same sampling frequency is used for a higher frequency wave, the sample points do not follow the oscillations. The features will not be correctly represented in the image.

- In practice, it is necessary to sample at 3-4x the resolution, to avoid numerical rounding errors.

Lecture 4 Scanning – number of grey levels


144


72


16

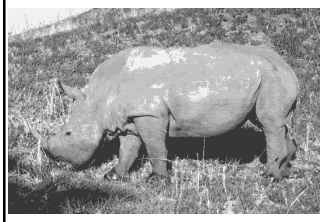
8

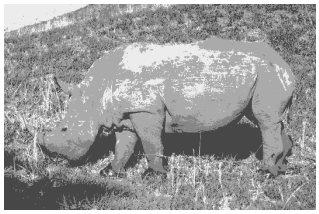
4


2

Lecture 4 Sampling - grey scale resolution

Film scanners generally scan into 8 bits (256 grey levels) or more. But if they are not set up correctly it is quite possible to end up with a digital image represented by far fewer grey levels. This can lead to degradation of the image and loss of resolution.

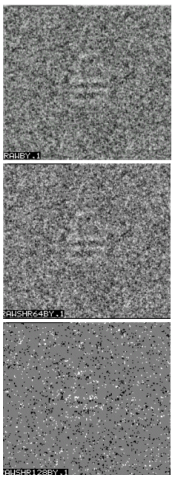

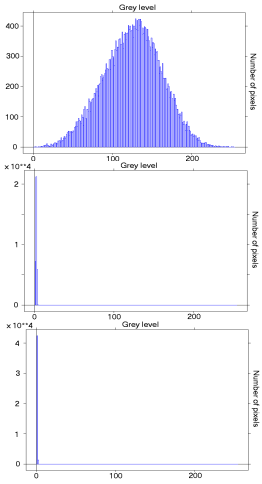

Scaled into 256 grey levels

5 grey levels

3 grey levels

Lecture 4

Statistical noise in low electron dose images

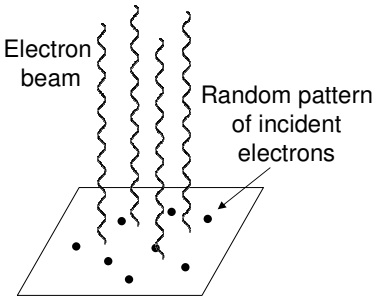

electron dose = average (N) ± √N

N = 100 electrons per unit area

108	90	103
102	95	114
94	105	89

√N / N = 10%

N = 1000 electrons per unit area

1025	1007	980
967	984	1016
1010	1046	964

√N / N = 3.3%

The signal to noise ratio improves by a factor of √N as the electron dose increases. However, for beam-sensitive specimens the dose must be kept low to avoid **radiation damage** to the specimen. Electrons can transfer energy to the specimen, breaking bonds and causing mass loss in biological molecules. For analysis, we assume that the image is the **sum** of the structure information plus random noise.

Lecture 4

Noise reduction by averaging

Raw images

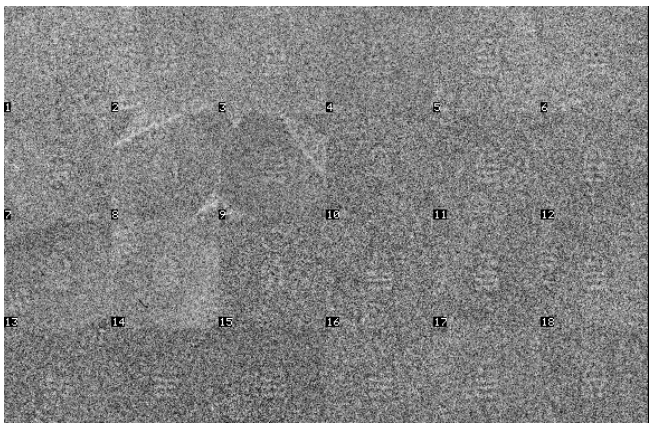

Averages of 2 5 10 25 200 images

Lecture 4

Variance

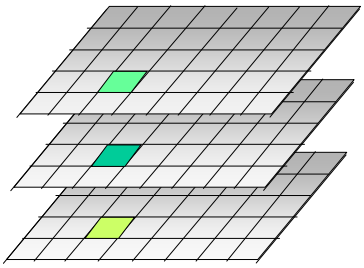

For a stack of aligned images, the variance can be calculated for each pixel, to give a map of variations between the images in the data set. This can help to assess the reliability of features seen on the average image, and can reveal if images of different structures are mixed up in the same data set.

The variance is determined for each pixel as the difference between the pixel value in a given image and the average value of that pixel in all the images. This difference is squared and the sum of these squares is calculated for all the images in the stack.

$$\text{Variance} = [1/(N-1)] \sum_{i,j} [P_i(r_j) - P_{av}(r_j)]^2$$

where $Pi(r_j)$ is the value of pixel j in image i and $P_{av}(r_j)$ is the average value of pixel j in all the images, for a set of N images.

Camera CCD

Successfully used in many TEM applications that are difficult or impossible to carry out without an online digital imaging system, (microscope autotuning, automated electron tomography, electron holography, protein electron crystallography and telemicroscopy)

- Broad dynamic range
- Linearity
- Low level of noise

Electron microscopy:
- No opening of the camera vacuum for film box exchange (can be a major source of water contaminants in a microscope column)
- Immediate quantitative feedback about the quality of both the sample and the data being collected rather than having to wait to develop and then to digitize the film

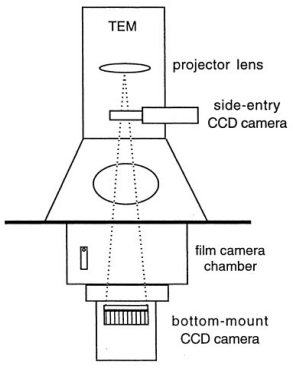

G. Y. FAN AND M. H. ELLISMAN *Journal of Microscopy, Vol. 200, Pt 1, October 2000, pp. 1–13.*

Film is still used in TEM applications

- Film
  - Satisfactory recording under a wide range of electron energies
- CCD
  - Difficulty of using CCDs for imaging with high energy electrons
  - Limited number of pixels offered by the currently available systems, as compared with that obtained by digitizing a TEM negative (small field of view)
- CCD for low-resolution studies (high SNR at low frequencies, better contrast, less images), film for high-resolution studies (high SNR at high frequencies, details better retrieved)

G. Y. FAN AND M. H. ELLISMAN *Journal of Microscopy, Vol. 200, Pt 1, October 2000, pp. 1–13.*

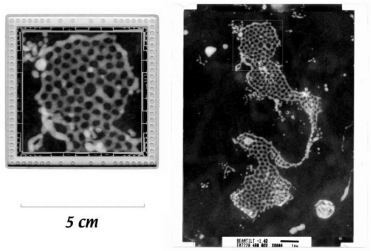

Fig. 2. A 2 k × 2 k CCD sensor (left) and a TEM negative film (right). The CCD (SITe SI424A) has a pixel size of 24 μm × 24 μm, and an imaging area of ~5 cm × 5 cm. The film (Kodak electron microscope film 4489) has an imaging area of ~7 cm × 9 cm. Because of the resolution difference, the CCD captures a smaller image area than its physical size suggests. The box on the negative shows the approximate area, as schematically overlaid on the CCD, that can be captured by the CCD if images are to be sampled at the same resolution. The specimen is a 1 μm section of selectively stained frog ganglia, showing the cis-face of the Golgi apparatus, taken at 400 kV.

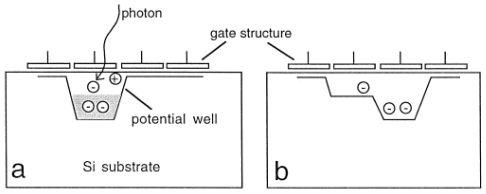

Fig. 3. Schematic illustration of CCD structure and operation. Front-side illuminated CCD is shown. In such a device, a photon must penetrate the electronic gate structure before it can interact with the Si substrate. The device can also be flipped over, the Si substrate thinned and anti-reflection coated to create a back-side-illuminated CCD, which has a considerably higher sensitivity.

When a photon enters the CCD, one or more electron-hole pairs may be created in the silicon substrate, depending on the energy of the photon. However, due to reflection and other energy competing processes in the substrate, a photon may not create an electron-hole pair even if it has enough energy to do so. The fraction that does is called the quantum efficiency of the CCD (a function of the wavelength of the incident photons).

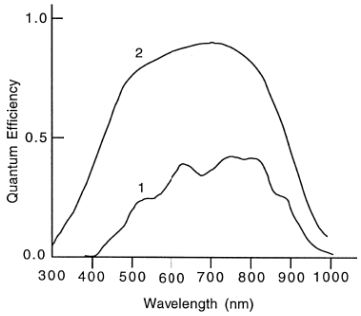

Fig. 4. Typical quantum efficiency curves of front-side-illuminated (1) and back-side-illuminated, anti-reflection-coated (2) scientific grade CCDs. An improvement in sensitivity by a factor of two can be easily achieved with the back-side-illuminated CCDs.

G. Y. FAN AND M. H. ELLISMAN *Journal of Microscopy, Vol. 200, Pt 1, October 2000, pp. 1–13.*

Electron-hole pairs are also created in CCDs due to thermal excitations, causing dark noise in the CCD. Dark noise accumulates with time, but can be reduced by cooling the CCD. Dark noise reduces by 50% for every ~7°C drop in temperature in silicon. At -30°C, dark noise can be reduced to a level of a few electron-hole pairs per pixel per second in a CCD.

G. Y. FAN AND M. H. ELLISMAN *Journal of Microscopy, Vol. 200, Pt 1, October 2000, pp. 1–13.*

Electrons generated in a pixel are collected in the potential well during integration (a). The amount of charge accumulated in a pixel is therefore proportional to the number of photons incident on that pixel during the period of integration. By coordinating the gate voltages (b), charges in one pixel can be transferred to an adjacent pixel, or any other pixel in a stepwise fashion. Typically, charges in any pixel have a fixed pathway to a readout register where the charge can be amplified and digitized. The number of transfers along the pathway will depend on the relative position of the pixel to the readout register. Due to the large number of transfers, particularly in large array CCDs, the charge transfer efficiency has to be very high to avoid charge loss. For scientific grade CCDs, the charge transfer efficiency reaches ~0.99999. Even so, it can be calculated that the charge loss can be as high as 4% for some pixels in for a 2 k x 2 k CCD.

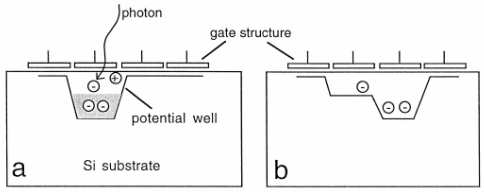

G. Y. FAN AND M. H. ELLISMAN *Journal of Microscopy, Vol. 200, Pt 1, October 2000, pp. 1–13.*

As ionizing particles, electrons with enough energy can also create electron-hole pairs in a CCD. Thus, CCDs can also be used for direct electron imaging. However, one incident electron generally creates too many electron-hole pairs in a CCD given the energy range typically involved in TEM. For example, a 100 keV electron will create in the order of 27 k electron-hole pairs in silicon. A 24 μm x 24 μm CCD pixel can have a full well capacity as high as ~500 k well electrons, whereas a 15 μm x 15 μm pixel has only about 80 k. Therefore, direct detection would result in an imaging system with a very high sensitivity but a very low dynamic range (e.g., a saturation level of 45 incident electrons at 100 keV (Roberts et al., 1982)). At higher electron energies, the dynamic range will be even lower. More importantly, the radiation damage to the CCD by the energetic electrons is a serious problem even at 100 keV. CCD imaging characteristics change markedly as a function of cumulative electron dose on the CCD (Roberts et al., 1982).

G. Y. FAN AND M. H. ELLISMAN *Journal of Microscopy, Vol. 200, Pt 1, October 2000, pp. 1–13.*

To avoid these problems, current CCD imaging systems for TEM applications employ a scintillator screen, which converts an electron image to a photon image. The photon image is then relayed to the CCD sensor either by a fibre-optic coupler or a lens.

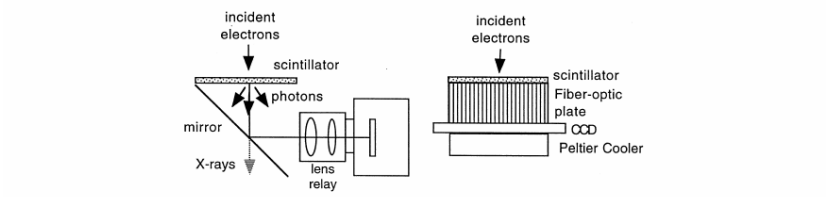

Fig. 6. CCD cameras in TEM. Instead of direct detection, a scintillator screen is used to convert an electron image to a photon image which is relayed, via a lens or an optical fibre plate, to a CCD. A bending of the optical path by 90° in the lens coupled system has the advantage of preventing X-rays from hitting the CCD, which would otherwise create bright spots on images. As the CCD sensor is cooled to ~ − 30 °C to reduce thermal noise, it has to be in a vacuum to avoid ice formation.

However, this introduces new problems. For example, scintillator may have a low photon yield, and/or a large point-spread function. The relay optics may further impose a resolution limit, relay efficiency, shading and geometrical distortion.

G. Y. FAN AND M. H. ELLISMAN *Journal of Microscopy, Vol. 200, Pt 1, October 2000, pp. 1–13.*

At present, the resolution of a CCD imaging system for TEM is limited to a large degree by the scintillator screen used. As expected, the dimension of the point-spread function increases drastically with electron energy. Even at 100 keV, the diameter of the point-spread function is in the order of 50 μm, whereas the pixel size of large format CCDs useful for electron microscopy is 24 μm or smaller. This means that the point spread function of the scintillator will cover several CCD pixels, therefore reducing the effective array size of the CCD. For example, a 1 k x 1 k CCD may only provide 500 x 500 independent pixels. The situation worsens rapidly with increasing energies.

Two remedies are apparent for this large point-spread function problem: (1) using a thinner scintillator screen, and (2) using a reducing optical relay. Both, however, lower the sensitivity of the imaging system.

G. Y. FAN AND M. H. ELLISMAN *Journal of Microscopy, Vol. 200, Pt 1, October 2000, pp. 1–13.*

CCD camera characterization

Parameters : resolution, sensitivity, linearity, dynamic range, detection quantum efficiency (DQE) and fixed-pattern noise. Some of these are interdependent, and it is possible and sometimes practiced to improve one at the expense of others.

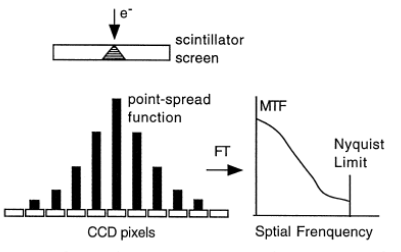

Fig. 9. Resolution of a CCD imaging system for TEM. Due to the point-spread function of the system (scintillator screen, optical relay and CCD itself), the signal due to a single incident electron covers several pixels. As a result, the maximum contrast achievable between two adjacent pixels is generally below 20%, as given by the MTF value at the Nyquist limit.

Resolution of a TEM digital imaging system is specified relative to its array size. Resolution can be measured in terms of the point-spread function, e.g. full width at half maximum in number of pixels, or the Fourier transform of it, which is called the modulation transfer function (MTF). Each stage of the imaging chain, i.e. the scintillating screen, the optical relay and the CCD sensor, has its own MTF and the overall MTF of the system is simply the product of all the MTFs of all stages. It is therefore often easier to work with MTF than the point-spread function.

G. Y. FAN AND M. H. ELLISMAN *Journal of Microscopy, Vol. 200, Pt 1, October 2000, pp. 1–13.*

Often, resolution is also expressed in terms of line-spread function, instead of point-spread function, as the line-spread function can be measured directly with the edge test (Dainty & Shaw, 1974). The two functions are related and knowing one allows the other to be derived. The Fourier transform of the line-spread function is also called MTF, although it is different from that derived from the point-spread function.

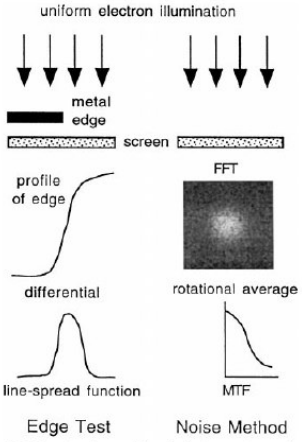

Fig. 10. Schematic of two useful methods of measuring resolution of a CCD imaging system: edge test and noise method. In the edge test method, the rise-width (10–90%) of the edge profile function or the full width at half maximum of the line-spread function can be used to characterize the resolution. With the noise method, the MTF can be obtained by rotationally average over the Fourier transform of the image of a uniform illumination.

G. Y. FAN AND M. H. ELLISMAN *Journal of Microscopy, Vol. 200, Pt 1, October 2000, pp. 1–13.*

Two useful methods of measuring the resolution of a TEM CCD imaging system are:

1 Edge test method (Dainty & Shaw, 1974). A straight metal edge that is thick enough to be opaque to incident electrons can be placed directly above the scintillating screen to measure the resolution of the imaging system. As the edge can be represented as a step function, differentiation of the image of the edge gives the line-spread function of the imaging system. As this function is typically noisy, many lines should be averaged along the edge to reduce noise. The drawback of this method is that the scattering of primary electrons and the generation of secondary electrons around the metal edge may affect the measurement, and the result is generally an over-pessimistic estimate of the MTF.

G. Y. FAN AND M. H. ELLISMAN *Journal of Microscopy, Vol. 200, Pt 1, October 2000, pp. 1–13.*

2. Noise method (Rabbani et al., 1987; De Ruijter & Weiss,1992). This method is based on the Fourier analysis of images of a uniform electron illumination. Due to the fluctuation of the number of electrons landing on a pixel, a uniform illumination actually represents a white noise input, which has a constant power spectrum over all Fourier frequencies. This constant spectrum will be attenuated by the MTF of the imaging system, so the Fourier transform of the image of a uniform illumination gives the MTF of the system. Because no special set-up or specimen is required to perform the measurement, this method is very easy to perform and can be done at any time. However, the accuracy of this method is influenced by the stochastic scattering of electrons in the scintillating screen, and the random generation and further scattering of photons in the scintillating screen. These random processes add noise to the image. As the added noise contains all Fourier frequencies, including high spatial frequencies, this method tends to give an over-optimistic estimate of the MTF. Simulations indicate that the discrepancy is smaller for scintillator screens that do not have a support substrate, such as a thin-foil screen (Fan et al., 1994).

G. Y. FAN AND M. H. ELLISMAN *Journal of Microscopy, Vol. 200, Pt 1, October 2000, pp. 1–13.*

Sensitivity: This is the minimum detectable signal in terms of the number of incident electrons.

Linearity: Relationship bteween output (image intensity in digital units) and the input (number of incident electrons). Due to the nature of CCD sensors, its output is strictly linear with the input up to the full well capacity of the CCD. Its linearity is therefore excellent up to the saturation level, provided that the readout circuits do not introduce non-linearities. This is a significant advantage over film, which typically has a more complex response curve.

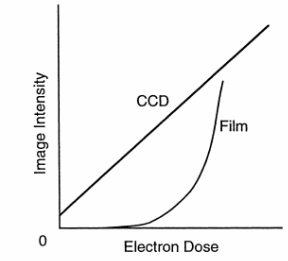

Fig. 11. The response of CCD is strictly linear up to the saturation level, whereas that of film is complex and more difficult to characterize.

G. Y. FAN AND M. H. ELLISMAN *Journal of Microscopy, Vol. 200, Pt 1, October 2000, pp. 1–13.*

Dynamic range : The ratio of the saturation level over the noise floor.

Detection quantum efficiency (DQE) : DQE characterizes the noise performance of an imaging system, and is defined as (Herrmann & Krahl, 1982):

$$\mathrm{DQE} = [(\mathrm{SNR})_o/(\mathrm{SNR})_i]^2$$

where (SNR)o and (SNR)i are the signal-to-noise ratio at the output and input, respectively.

Supposing one incident electron causes a pixel intensity increase, on the average, of g digital units, which can be greater or smaller than 1. With a uniform electron illumination, the average number of electrons per pixel, N, can be calculated from the image mean, M, by

$$N = M/g$$

and for a Poisson process:

$$(\mathrm{SNR})_i = N^{1/2}$$

G. Y. FAN AND M. H. ELLISMAN *Journal of Microscopy, Vol. 200, Pt 1, October 2000, pp. 1–13.*

The standard deviation (σ) of the image can also be measured, so (SNR)o can be calculated easily:

$$(\mathrm{SNR})_o = M/\sigma$$

This gives:

$$\mathrm{DQE} = M^* g/\sigma^2$$

G. Y. FAN AND M. H. ELLISMAN *Journal of Microscopy, Vol. 200, Pt 1, October 2000, pp. 1–13.*

DQE is a function of electron dose. At low dose levels of a few incident electrons per pixel, DQE of a TEM CCD imaging system is typical low due to the readout noise of CCD, but it improves rapidly with electron dose to a stable level. At dose levels of 100 electrons per pixel and higher, the improvement of DQE with electron dose becomes insignificant.

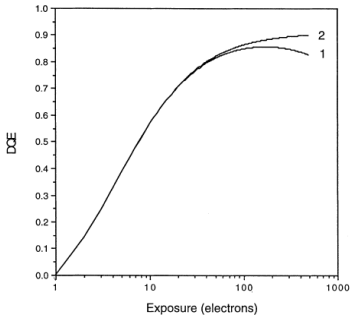

Fig. 12. DQE of a CCD imaging system for TEM is typically low at low dose levels due to the readout noise in the CCD electronics, but increases rapidly with dose and plateaus at the dose level of ~100 electrons pixel^{-1}. DQE goes down at higher dose levels if gain-normalization of images is not done properly (curve 1). DQE approaches a constant (curve 2) if the gain reference (flat field) and dark noise images used for gain-normalization, obtained with a uniform illumination and no illumination, respectively, are averaged over many frames to avoid gain variations.

G. Y. FAN AND M. H. ELLISMAN *Journal of Microscopy, Vol. 200, Pt 1, October 2000, pp. 1–13.*

For an ideal system, DQE should be unity, which means that the system itself is noise free. In practice, a system always contributes a certain amount of noise, so its DQE is always less than unity. The main sources of noise in a CCD-based TEM digital imaging system are: readout noise from the electronics (amplification, A/D conversion, etc.), thermal noise in the CCD and pulse-width distribution in the scintillating screen. Readout noise is at a fixed level, meaning it is independent of the integration time or electron dose. It is likely to be the dominant noise for low dose imaging conditions. Thermal noise is due to thermal excitations in CCDs, as discussed earlier, and the resulting dark noise accumulates with time. As thermal noise accumulates with time, it is likely to be the dominate noise for long integration times. The pulse width distribution reflects the fact that the electron-photon conversion in the scintillator is a random process, and the number of photons generated due to each incident electron is not a constant but follows a probability distribution called pulse-width distribution. Thus, even if the readout noise and thermal noise could be completely eliminated from the CCD, system DQE would not be unity simply because of this conversion process. This type of noise can be reduced by selecting a scintillating material that has a narrower pulse width distribution. Crystalline YAG screens, for example, are generally better than powder phosphor screens in this respect.

G. Y. FAN AND M. H. ELLISMAN *Journal of Microscopy, Vol. 200, Pt 1, October 2000, pp. 1–13.*

Fixed-pattern noise:

Another unique aspect of large format CCD imaging systems is that, owing to the large number of pixels contained in a CCD sensor, some defects are unavoidable even in the highest grade CCDs. These defects include individual or groups of pixels having an abnormal response, i.e. they may have a higher level of dark noise, or may be brighter or dimmer than the rest of the pixels under a uniform illumination. These give rise to a fixed-pattern noise in an image. In addition, the non-uniformity in the scintillator screen, defects in the fibre-optic coupler (which often form chicken-wire patterns) or vignetting of the lens relay also contribute to the fixed-pattern noise. Fortunately, this problem can be very effectively corrected by a simple gain-normalization procedure.

G. Y. FAN AND M. H. ELLISMAN *Journal of Microscopy, Vol. 200, Pt 1, October 2000, pp. 1–13.*

This involves acquiring a dark noise image (with no illumination), denoted by D, and an image of a uniform illumination, denoted by G, which are used as the gain reference (sometimes called flat-field). Then a raw image, denoted by Ir, can be gain-normalized to yield the correct image, denoted by I, by applying a pixel-wise operation given by:

$$I = C^{*}(I_{\mathrm{r}} - D)/(G - D)$$

where C is a constant and should be set to be the mean of (G - D) to preserve image intensity. To avoid fluctuations in the dark noise image and in the gain reference, both D and G should be averaged over many frames before using. Not doing so will degrade the DQE of the system, particularly at high electron dose (Ishizuka, 1993).

G. Y. FAN AND M. H. ELLISMAN *Journal of Microscopy, Vol. 200, Pt 1, October 2000, pp. 1–13.*

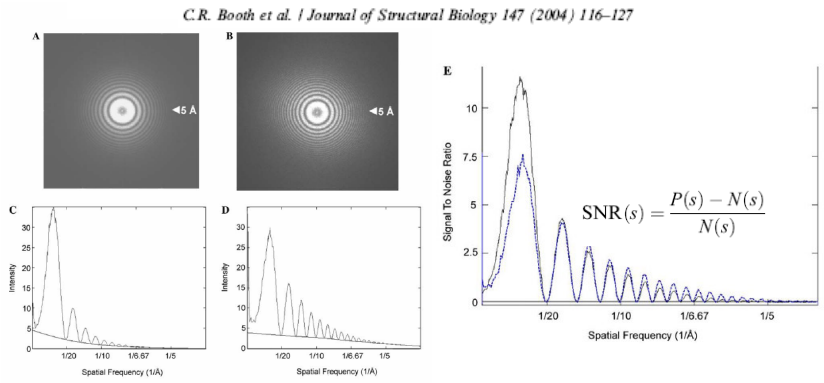

Fig. 2. Characterizing the CCD Camera. Images of amorphous carbon film recorded on CCD and photographic film followed by digitization in a Zeiss scanner. (A) 2-D power spectrum calculated from amorphous carbon film imaged on CCD. (B) 2-D power spectrum calculated from amorphous carbon film imaged with photographic film and scanned using a Zeiss scanner at 7 μm. (C–D) 1-D power spectrum and noise profile estimate calculated by rotationally averaging (A) and (B), respectively, and fitting a line through the zeroes of the contrast transfer function. Signal-to-noise ratio (SNR) comparison between images of amorphous carbon film collected on CCD and film is shown in (E). In a solid line is the SNR calculated from data collected on CCD. Shown in a dotted line is the SNR calculated from digitized data collected on film.

SNR of the CCD data is better than the SNR of the photographic film data at low spatial frequencies. At 2/5 Nyquist frequency the SNR between the two datasets is equivalent and at higher spatial frequencies the SNR of film data is better than the SNR of CCD data. The analysis showed the same trend regardless of defocus values or microscope magnification.

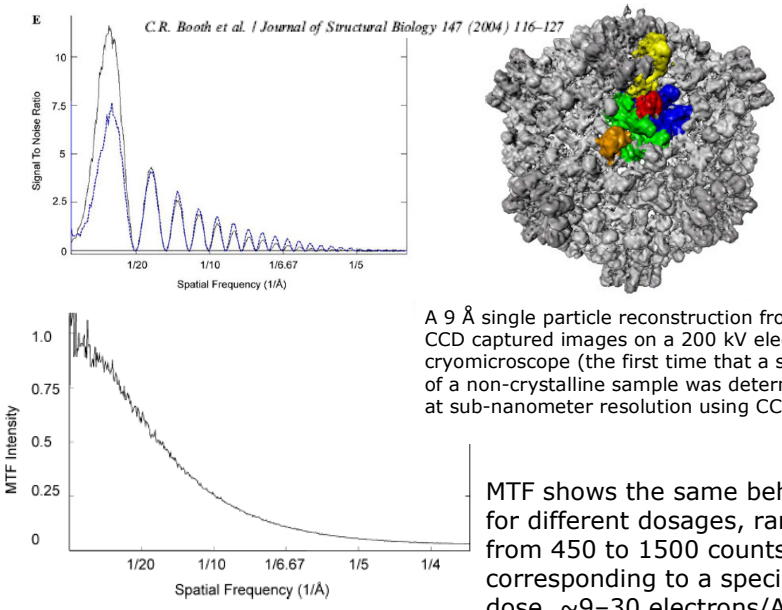

Fig. 3. Estimating the MTF of the CCD Camera. The CCD was evenly illuminated in the absence of sample to collect images of white noise which were used to estimate the MTF using the Noise method of (de Ruijter and Weiss, 1992).

A 9 Å single particle reconstruction from 4kx4k CCD captured images on a 200 kV electron cryomicroscope (the first time that a structure of a non-crystalline sample was determined at sub-nanometer resolution using CCD camera)

MTF shows the same behavior for different dosages, ranging from 450 to 1500 counts/pixel corresponding to a specimen dose, ~9–30 electrons/A², typically used for imaging ice embedded single particles.

Film continues to provide greater SNR at spatial frequencies greater than 2/5 Nyquist frequency and a larger field of view than the CCD camera, necessary for collecting the quality and quantity of data necessary for structures at better than 9 Å resolution.

There is still signal beyond 9 Å though the SNR is relatively low. One could use more particles to build up statistics in order to retrieve structural information beyond 2/5 Nyquist frequency. This would require a more powerful image reconstruction algorithm. Alternatively, one can use a higher magnification, so that 2/5 Nyquist frequency would correspond to a higher spatial frequency value. This would result in a smaller area and thus fewer particles per CCD frame. In either approach, one would need more data. An automated image acquisition is required (Carragher et al., 2004).

Table 3
Relationship of effective microscope magnification, sampling value, specimen area and 2/5 Nyquist frequency relative to those at 82 800× magnification

Effective Microscope magnification	Å/pix	Dimension of CCD frame on specimen (nm)	CCD frame area compared to 82 800 (%)	2/5 Nyquist (Å)
55 200	2.71	1110	225.00%	13.55
69 000	2.17	886	144.00%	10.84
82 800	1.81	738	100.00%	9.03
110 400	1.35	554	56.25%	6.77
138 000	1.08	443	36.00%	5.42
207 000	0.72	295	16.00%	3.61

Optimization of the scintillator for 300 kV has resulted in a superior point spread function. For the first time, we see that at 300kV the MTF of the CCD camera (4k x4k) may not be the major factor limiting detectable signal to at least half of the Nyquist frequency.

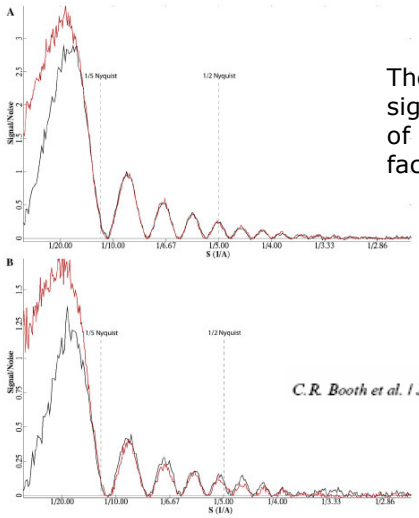

The fall-off of detectable signal is caused by a variety of different experimental factors and specimen motion.

C.R. Booth et al. / Journal of Structural Biology 156 (2006) 556–563

Fig. 5. Comparing the CCD camera to film. Comparing the SNR curve of CCD (red), at an effective magnification of 112 000, and FILM (black), at an effective magnification of 80 000, at a defocus of 0.59 μm and estimated using twenty-eight 512 × 512 pixel boxes. Shown in (A) from images collected at 35 electrons/Å^2 (corresponding to a O.D. on film of 0.55) and (B) at 15 electrons/Å^2 (corresponding to an O.D. of film of 0.2).

Sélection des particules (*Helix pomatia*)

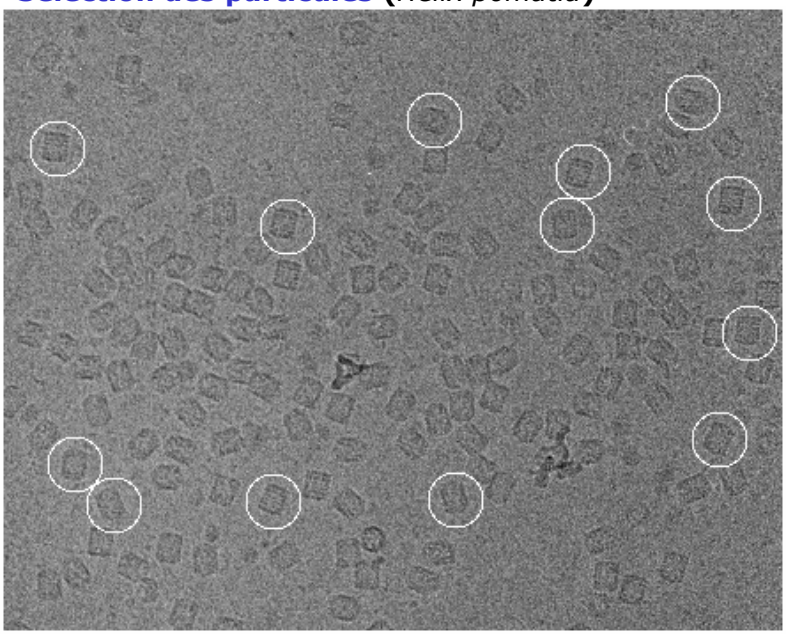

Normalisation du contraste

Soustraction de la moyenne et division par l'écart type

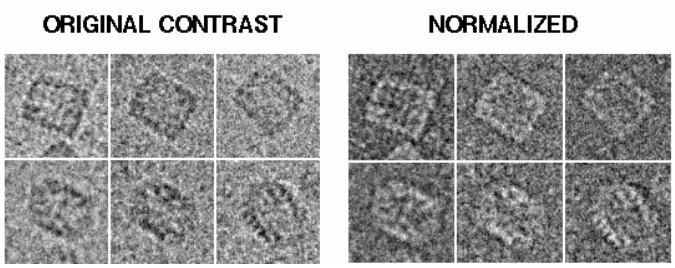

Alignement et fonctions de corrélation

Corrélation croisée 2D

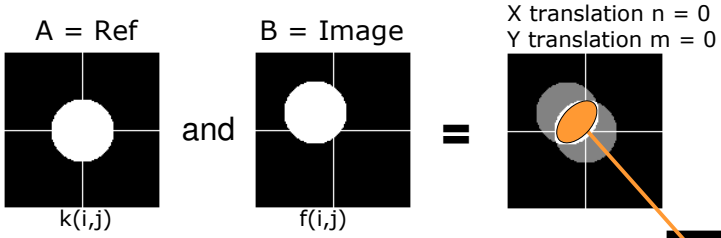

Puis B est translaté et à chaque position de B en X et Y un nouveau coefficient de corrélation est calculé.

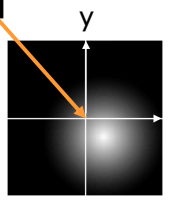

$\Sigma\Sigma$ k(i,j) . f(i+n,j+m)

Le résultat final est une carte bidimensionnelle dont la taille correspond à celle des images d'origine et qui possède un pic de corrélation qui correspond à la translation de B pour laquelle les deux disques se superposent parfaitement.
La position du pic par rapport à l'origine (centre de la carte) correspond au vecteur de translation à appliquer pour recentrer l'image B par rapport à l'image A (x +15 , y -15).

Alignement et fonctions de corrélation

Fonction d'Auto-Corrélation = FAC

C'est la corrélation croisée d'une image avec elle-même

Image 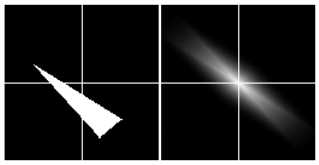 ACF

La FAC est une fonction "Centrée"
Fmax toujours à la position X = 0 et Y =0

La FAC est une fonction "Paire"
F(x,y) = F(-x,-y)

Alignement et fonctions de corrélation

Corrélation croisée angulaire

Une image B (supposée centrée) est placée sur une image de référence, et pour chaque rotation de B, on mesure leur coefficient de corrélation.

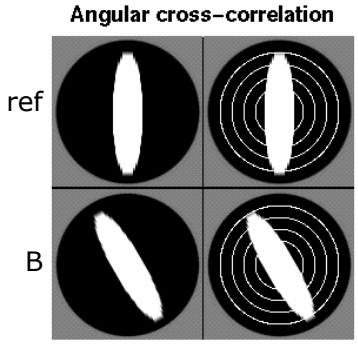

La corrélation est calculée sur une série de rayons et la valeur globale est inscrite en fonction de l'angle de rotation.

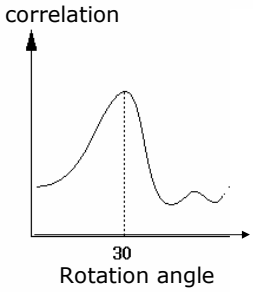

Alignement et fonctions de corrélation

Exemple d'alignement sur une référence

Référence image B

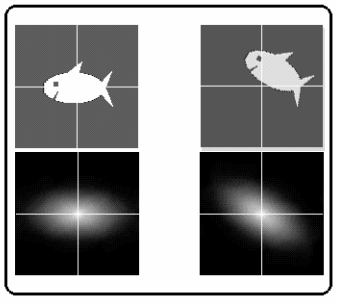

FAC ref FAC B

On calcule les FACs des images pour obtenir une représentation centrée et reflétant partiellement la structure des particules.

Corrélation croisée angulaire des FACs

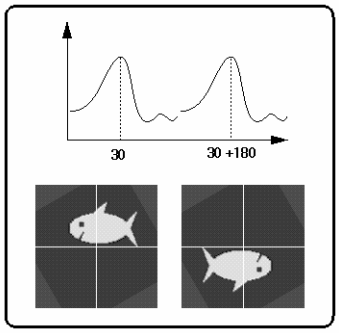

Mais comme les FACs sont des fonctions paires, il y a une ambiguïté de 180° sur l'angle de rotation qu'on trouve en calculant leur corrélation croisée angulaire.

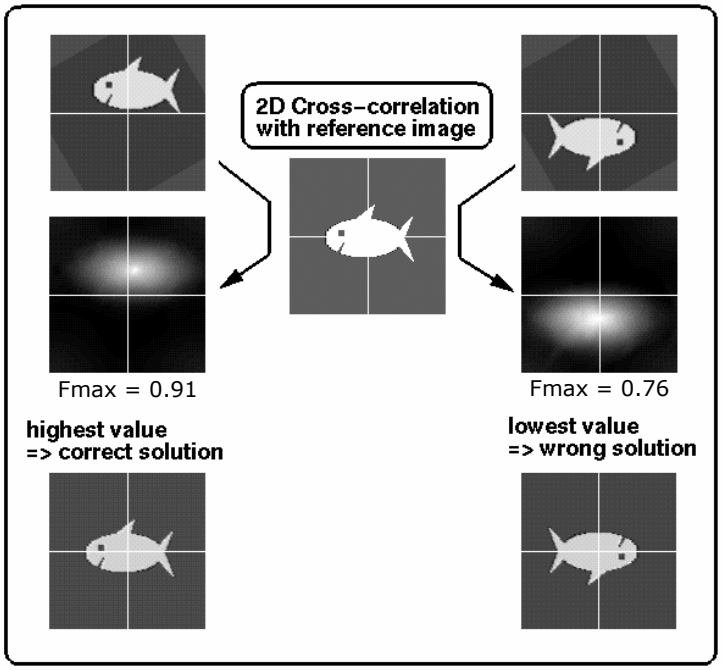

D'autres méthodes d'alignement ont été proposées pour minimiser l'influence de l'image de référence.

"Reference free" iterative alignment (Penczek *et al*., 1992) **:**
1) Ici deux images sont prises au hasard, alignées et leur moyenne est alors utilisée comme nouvelle référence pour aligner une troisième image. Le processus se reproduit itérativement jusqu'à ce que toutes les images soient alignées.

2) Pour minimiser l'influence de l'ordre dans lequel les images ont été choisies pendant l'alignement, on repart ensuite à l'envers, en réalignant la première image et en la réalignant sur (Moyenne totale - l'image 1). Puis la seconde image est réalignée sur (Moyenne totale - l'image 2), etc …

3) Le processus entier est recommencé à nouveau sur les images issues de ce premier cycle d'alignement (étapes 1 et 2), jusqu'à ce qu'aucune amélioration ne soit constatée d'un cycle au suivant.

"multi-reference alignment" et d'autres méthodes d'alignement utilisent la classification en parallèle du processus d'alignement.

Helix pomatia side views
before alignment

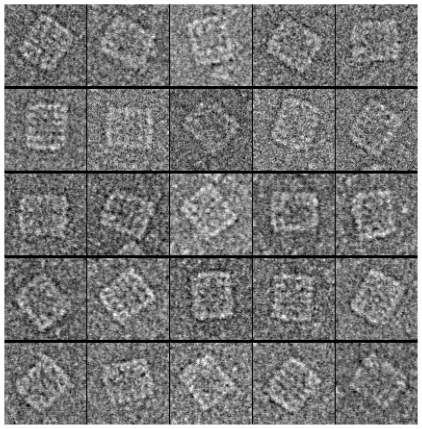

Helix pomatia side views
after alignment

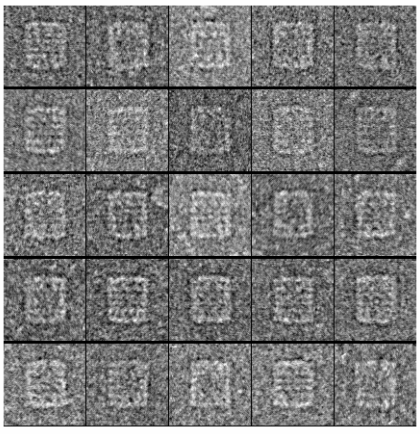

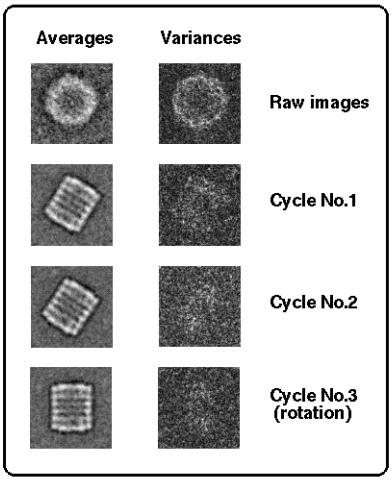

Classification

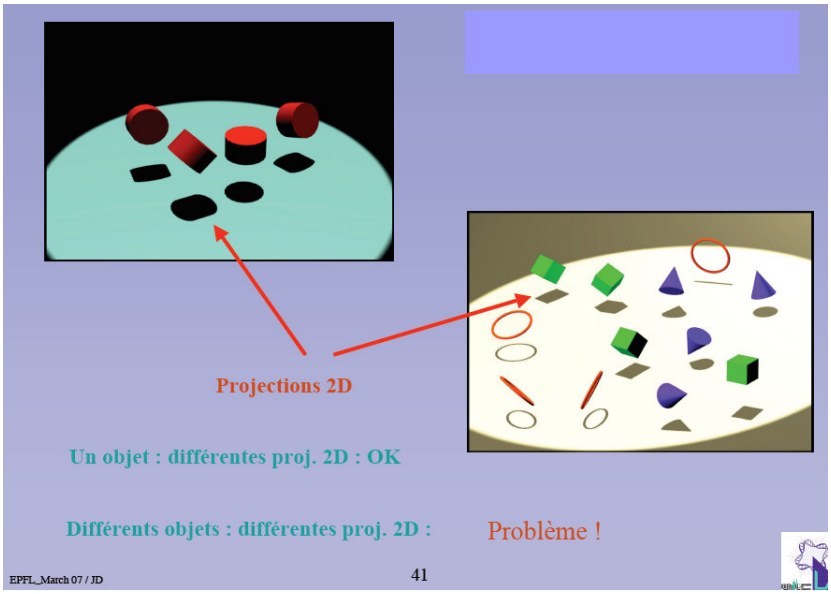

Brétaudière JP and Frank J (1986) Reconstitution of molecule images analyzed by correspondence analysis: A tool for structural interpretation. *J. Microsc.* **144**, 1-14.

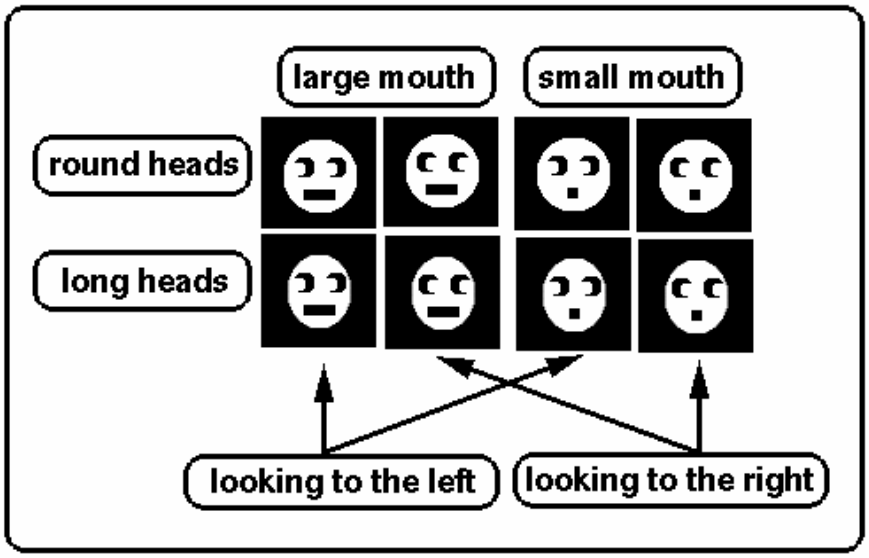

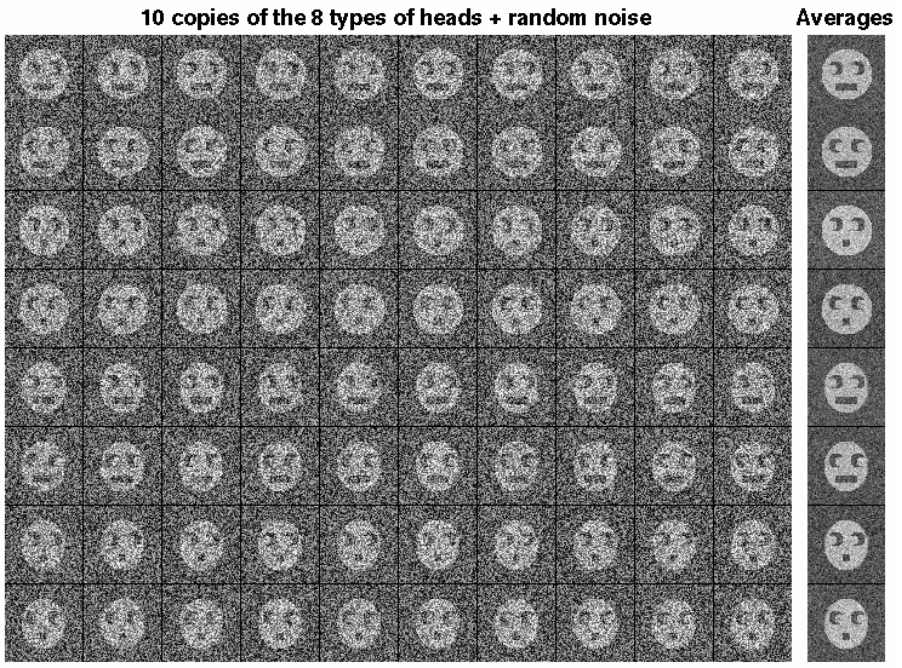
10 copies of the 8 types of heads + random noise
Averages

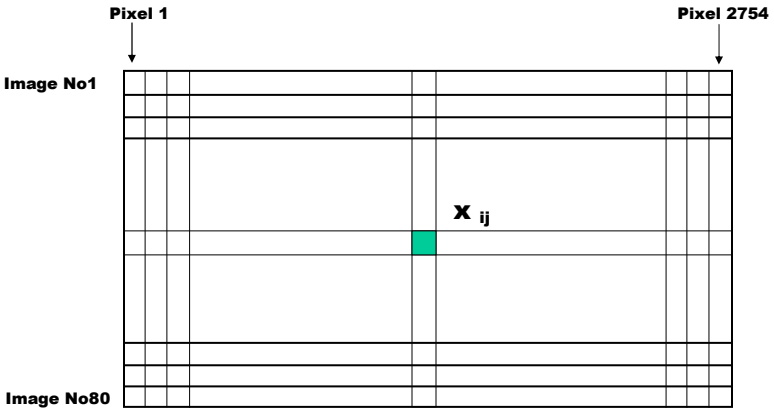
Pixel 1
Pixel 2754
Image No1
x ij
Image No80

La diagonalisation de la matrice carrée **T = X'X** permet de déterminer la plus grande direction d'extension de nos données (nuage de points) dans l'espace multi-dimensionnel. Cette direction d'extension correspond à la plus grande « variation » ou « tendance » au sein de nos données. C'est l'axe factoriel N°1 dont l'amplitude est caractérisé par la valeur propre λ_1. On effectue alors un changement de repère pour déterminer la position de chacune de nos données (images) par rapport à cet axe factoriel. Puis, on recherche la seconde plus grande direction d'extension « orthogonale » à la première pour définir l'axe factoriel N°2 caractérisé par une amplitude de λ_2. Le fait que les axes factoriels N°1 et 2 soient orthogonaux, indique qu'ils caractérisent des variations indépendantes (non-corrélées). On exprime ainsi par ordre décroissant toutes les variances indépendantes de nos données sur les axes factoriels N°1, 2, 3, 4 ,etc …

Méthode de la dragée

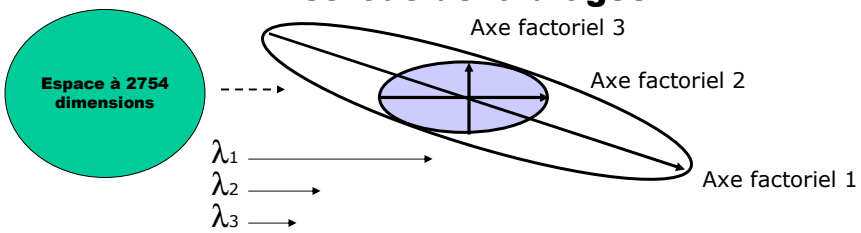

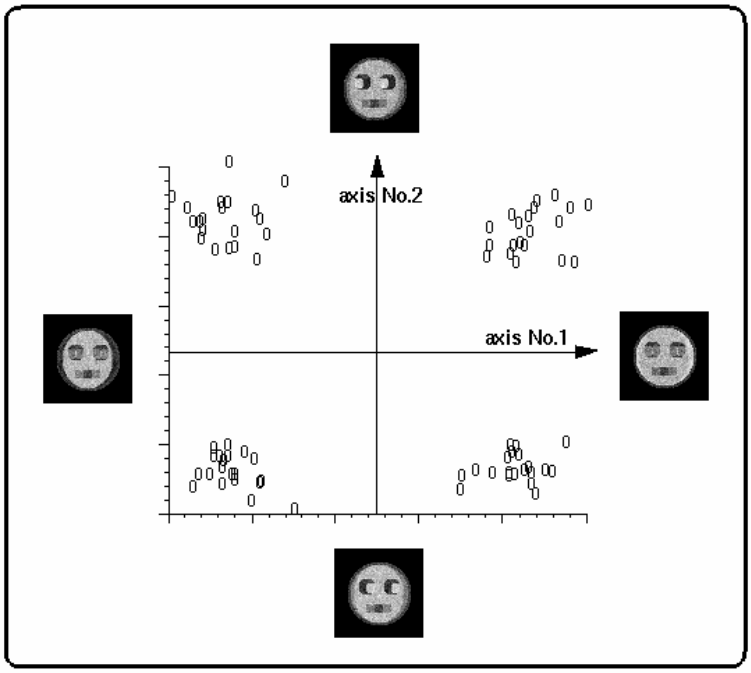

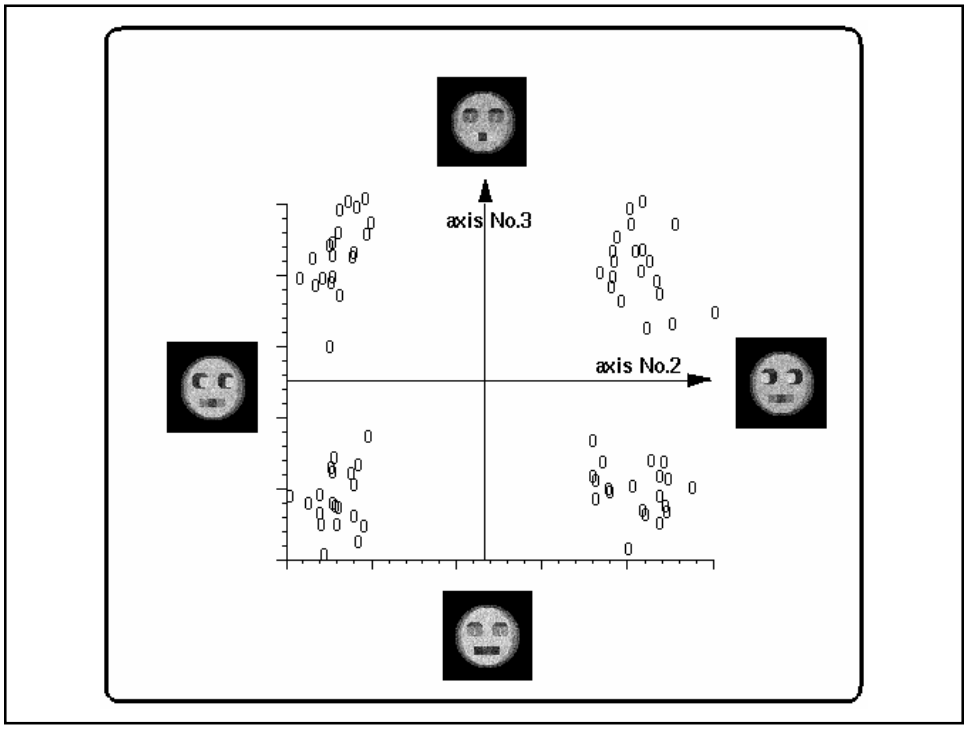
axis No.3
axis No.2

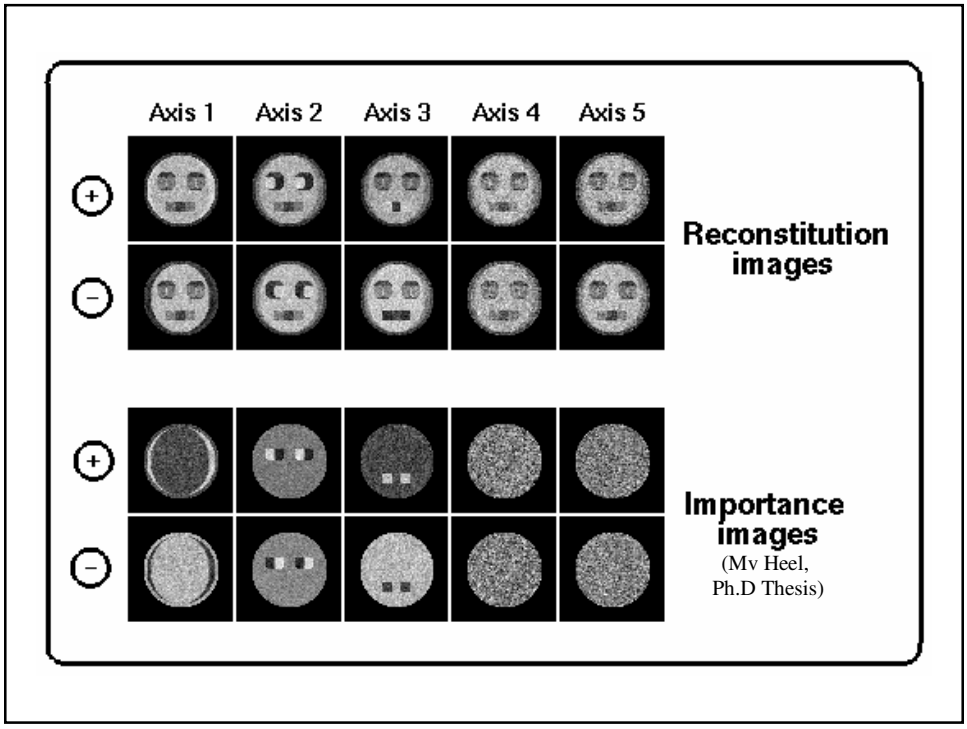
Axis 1
Axis 2
Axis 3
Axis 4
Axis 5
+
−
Reconstitution images
+
−
Importance images
(Mv Heel, Ph.D Thesis)

Méthodes par partition: *e.g.* "Moving seeds" method

Diday E (1971) La méthode des nuées dynamiques. *Rev. Stat. Appl.* **19**, 19-34.

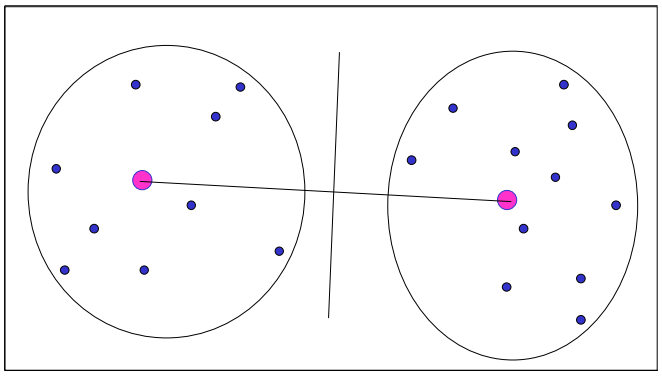

Deux images prises au hasard servent de centres d'agrégation pour la partition. Les centres de gravité de chaque classe servent de nouveaux centres d'agrégation pour un nouveau cycle de partition. Arrêt lorsque les centres d'agrégation ne bougent plus d'un cycle à l'autre, ou après un nombre déterminé d'itérations.

Classification Ascendante Hiérarchique

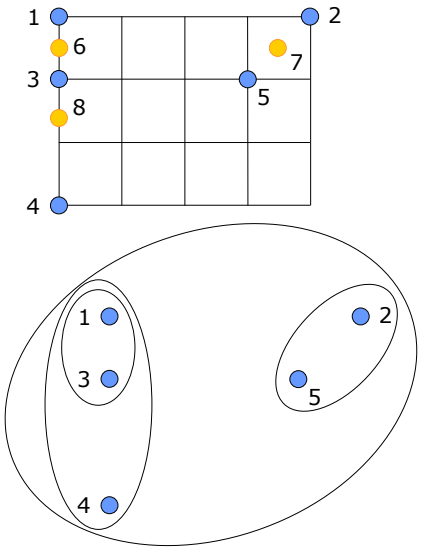

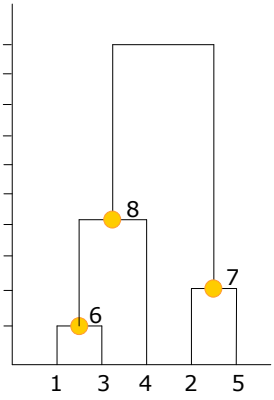

HIERARCHICAL ASCENDENT CLASSIFICATION

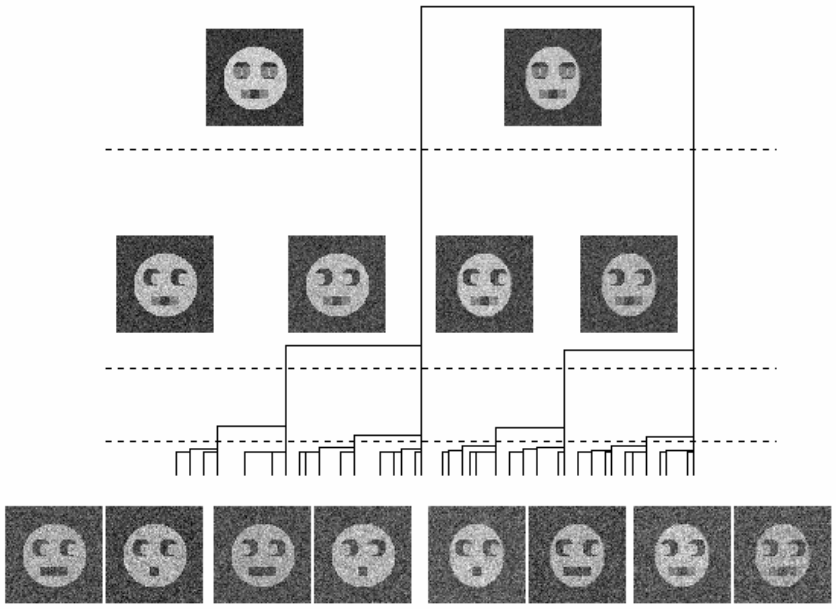

Hétérogénéité

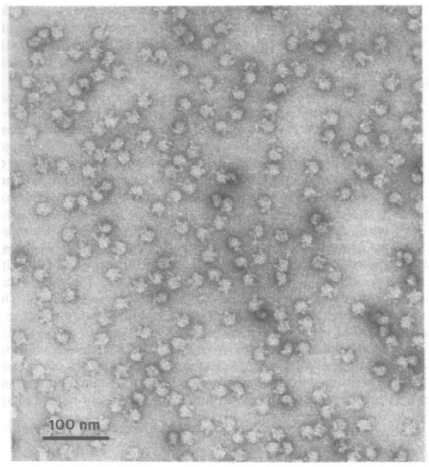

FIG. 1. Electron micrograph of 50S ribosomal subunits.

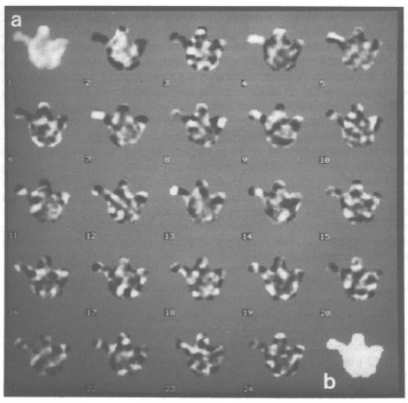

FIG. 4. (a) The data set of 1956 aligned images is decomposed by correspondence analysis into eigenimages which represent the principal components of interimage variation. The first eigenimage points to the center of mass of the full data set. The second, third, fourth, and fifth eigenimages describe 6.2, 4.9, 1.9, 1.7, and 1.4% of the total interimage variance, respectively, whereas the twenty-fourth eigenimage describes only 0.8%. All 24 eigenimages account for 34.2% of the total interimage variance. (b) Binary mask generated from the total sum of 1956 aligned images, defining the image area active in correspondence analysis. The total sum is a blurry image which indicates those regions within the image area within which the pixels belong (usually) to the molecule and not to negative stain or carbon support film.

Harauz et al. *Meth Enzymol*, pp. 35-49, 1988

Harauz et al. *Meth Enzymol*, pp. 35-49, 1988

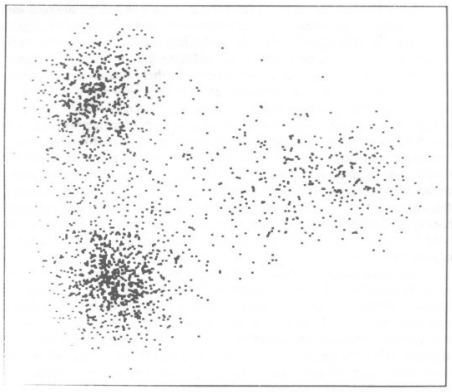

FIG. 5. Correspondence analysis map of factorial coordinates 3 (vertical axis) versus 2 (horizontal axis). Each image is represented as a dot, and the entire population forms a cloud. There are two major subpopulations, blending into a more diffuse third group.

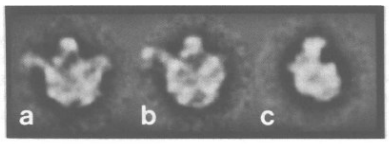

FIG. 6. Classes representative of the three groups seen on the correspondence analysis map.

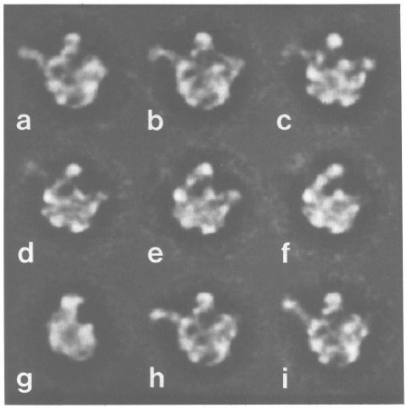

FIG. 7. Partitioning of the population of 1956 images into classes; those with a low intraclass variance are selected for final analysis. The two crown views (a and b) are predominant (forming about two-thirds of the classes). The remaining classes appear to be views intermediate between the crown and kidney (c–g). In the final two crown classes (h and i), the L7/L12 stalk lies in different positions, spanning a distance of over 2 nm.

References

Carragher B, Kisseberth N, Kriegman D, Milligan RA, Potter CS, Pulokas J, Reilein A (2000) Leginon: an automated system for acquisition of images from vitreous ice specimens. *J. Struct. Biology* 132, 33-45.

Potter CS, Chu H, Frey B, Green C, Kisseberth N, Madden TJ, Miller KL, Nahrstedt K, Pulokas J, Reilein A, Tcheng D, Weber D, Carragher B. (1999) Frank, J. (1975). Averaging of low exposure electron micrographs of nonperiodic objects. *Ultramicroscopy* 1, 159-162.

Frank, J., and Al-Ali, L. (1975). Signal-to-noise ratio of electron micrographs obtained by cross-correlation. *Nature* 256, 376-378.

Frank J. (1996) Three-dimensional microscopy of macromolecular assemblies. *Academic Press*, San Diego.

Frank J. (1990) Classification of macromolecular assemblies studied as 'single particles'. Quart. Rev. Biophys. 23, 281-329.

Henderson, R., and Glaeser, R.M. (1985). Quantitative analysis of image contrast in electron micrographs of beam-sensitive crystals. *Ultramicroscopy* 16, 139-150.

Henderson, R. (1995). The potential and limitations of neutrons, electrons and X-rays for atomic resolution microscopy of unstained biological molecules. Quart. Rev. Biophys. 28, 171-193.

Saxton, W.O. (1994) Accurate alignment of sets of images for super-resolving applications, *J. Microsc*. 174, 61-68.

van Heel, M. (1989). Classification of very large electron microscopical image data sets. *Optik* **82**, 114-126